JBUON 2019; 24(6): 2493-2501
ISSN: 1107-0625, online ISSN: 2241-6293 • www.jbuon.com
Email: editorial_office@jbuon.com

ORIGINAL ARTICLE

An isoliquiritigenin derivative inhibited myeloma cells' proliferation and its interactions with human serum albumin

Wei Cao[1]*, Le Fang[2]*, Zhaoxia Zhang[3], Jianing Xi[4]

[1]Clinical Laboratory, Beijing Rehabilitation Hospital, Capital Medical University, Beijing 100144, China; [2]Clinical Laboratory, 521 Hospital of Ordnance Industry, Xi'an 710065, China; [3]Clinical Laboratory, First Affiliated Hospital of Xinjiang Medical University, Urumqi 830054, China; [4]Beijing Rehabilitation Hospital, Capital Medical University, Beijing 100144, China.

*Wei Cao and Le Fang contributed equally to this work.

Summary

Purpose: *In this paper, we reported an isoliquiritigenin (ISL) derivative, namely* ***1b****, which reduced the interleukin-6 (IL-6) expression in RPMI-8226 and CZ-1 cancer cells, thus leading to the cell death.*

Methods: *The growth inhibitory effect of ISL and its derivative* ***1b*** *was measured on RPMI-8226 and CZ-1 cancer cells. To explore the mechanism of cancer cells death, ISL and* ***1b*** *were used to induce CZ-1 cells apoptosis, which was then examined by using the Annexin V-FITC/propidium iodide (PI) kit. Human IL-6 ELISA Kit (ab46042) was used for the quantitative measurement of IL-6 protein in cell culture medium from CZ-1 control cells, or cells treated with ISL and* ***1b****.*

Results: ***1b*** *could induce CZ-1 cells apoptosis in a dose-dependent manner. The pharmacokinetic property of* ***1b*** *was explored by the interaction of* ***1b*** *with human serum albumin (HSA). Binding parameters indicated that* ***1b*** *bound to HSA with binding affinity of the order 10^4 L/mol, a moderate binding constant, suggesting* ***1b*** *could be stored and carried by the protein. Moreover, the binding reaction between HSA and* ***1b*** *was exothermic, hydrogen bonds and hydrophobic interactions were the predominant intermolecular forces to stabilize the formed* ***1b*** *-HSA complex. Site markers competitive experiments revealed that* ***1b*** *bound to both site I and site II of HSA simultaneously. Collectively, our data suggested that* ***1b*** *could be transferred by HSA to its target for myeloma cell growth inhibitory effects.*

Conclusions: *Our data suggested that* ***1b*** *could be transferred by HSA to its target for myeloma cell growth inhibitory effects.*

Key words: *isoliquiritigenin, human serum albumin, interaction, anticancer, binding*

Introduction

Isoliquiritigenin (ISL) (Figure 1A), a simple chalcone-typed flavonoid structure, exists in licorice and vegetables [1]. Increasing evidences has demonstrated that ISL possesses a variety of biological and pharmacological properties [2], including antioxidant [3], anti-inflammatory [4], antiplatelet [5], antipepticulcer [6], antiangiogenic [7] and antitumor activities [8-10]. Especially, ISL has been shown to possess significant anticancer activity against glioma cells *via* inhibiting the topoisomerase I activity [11]. Moreover, ISL was reported to induce G2/M phase arrest and apoptosis in ovarian cancer cells [12]. In addition, ISL displayed a vital inhibitory effect on breast cancer through directing binding to GRP78 to regulate β-catenin pathway [13]. Recently, ISL was reported to reduce the IL-6 expression in RPMI-8226 and CZ-1 cancer cells, thus inhibiting their proliferation *in vitro* [14]. Based on these results, our group has made extensive modifications on ISL, leading

Corresponding author: Jianing Xi, PhD. Beijing Rehabilitation Hospital, Capital Medical University, Xixia Zhuang, Badachu Rd, Shijingshan, Beijing, China.
Tel/Fax: +86 18811135612, Email: jianingxi66@163.com
Received: 25/06/2019; Accepted: 21/07/2019

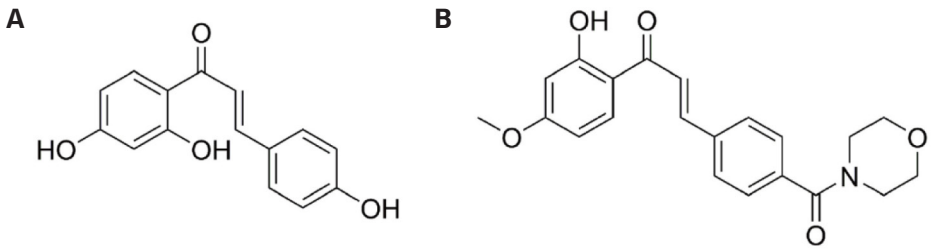

Figure 1. Chemical structures of ISL **(A)** and its derivative **(B)**.

to the discovery of one ISL derivative (Figure 1B) with an improved anticancer activity.

Though **1b** has been shown to exhibit an excellent anticancer activity, the pharmacokinetic behavior of the compound remains unknown. To obtain the preliminary pharmacokinetic behavior of **1b**, we studied its interaction with human serum albumin (HSA).

HSA is a key carrier protein in plasma [15]. When a drug or small molecule binds to HSA, it could be transported to its target. Given the importance of HSA function, a thorough investigation of the binding profile of a bioactive molecule with HSA is beneficial to understanding of the absorption, distribution, metabolism and excretion properties of the compound [16]. An analysis of the crystal structure of HSA revealed that the protein contains three similar domains (I, II and III) and each domain has two subdomains (A and B) [17]. The regions of drug-binding site in albumin are located in subdomains IIA or IIIA, also known as Sudlow I or Sudlow II, respectively. HSA has only one tryptophan residue Trp-214, locating in Sudlow I. Ibuprofen and warfarin have long been considered as stereotypical ligands binding to Sudlow's site I and II, respectively [18,19], which could be used to identify the binding pocket for a bioactive compound.

In this paper, we reported the biological evaluation of **1b** as an anticancer agent, which was found to reduce the IL-6 expression in MM cells. The fluorescence spectroscopic methods were then employed to investigate the binding profile of **1b** to HSA under physiological conditions, with the aim to investigate the preliminary pharmacokinetic characteristics of **1b**.

Methods

HSA, warfarin and ibuprofen were obtained from Sigma-Aldrich with purities of more than 95% (St. Louis, MO, USA). Triisopropyl ethyl sulfonyl (Tris), NaCl, HCl, and C_2H_5OH were of analytical purities and used as received. HSA was dissolved in Tris-HCl buffer solution (0.05 M Tris, 0.15 M NaCl, pH=7.4) to fix a concentration of 1.0×10^{-5} M. ISL derivative **1b** was dissolved in ethanol to prepare a stock solution of 5×10^{-3} M. Samples mass was weighed on a microbalance with a resolution of 0.1 mg. All other chemicals and solvents were commercially available, and were used without further modifications.

Cell lines and culture

The human cancer cell lines RPMI-8226 and CZ-1 were obtained from the American Type Culture Collection (ATCC, Manassas, VA, USA). All cells were cultured in Roswell Park Memorial Institute 1640 (RPMI 1640) (Gibco, Rockville, MD, USA) supplemented with 10% fetal bovine serum (FBS) (Gibco, Rockville, MD, USA), 100 U/mL penicillin, 100 µg/mL streptomycin at 37°C, in a humidified atmosphere containing 5% CO_2.

*Synthesis of compound (E)-1-(2-hydroxy-4-methoxyphenyl)-3-(4-(morpholine-4-carbonyl)phenyl)prop-2-en-1-one (**1b**)*

Compound **1b** was synthesized according to the literature [14]. M.p. 159-160°C. ^{1}H NMR (400 MHz, $CDCl_3$) δ 13.34 (s, 1H), 7.84 (d, *J*=15.5 Hz, 1H), 7.82 (d, *J*=8.7 Hz, 1H), 7.68 (d, *J*=8.1 Hz, 2H), 7.62 (d, *J*=15.5 Hz, 1H), 7.49 (d, *J*=8.2 Hz, 2H), 6.51 (dd, *J*=8.0, 2.5 Hz, 1H), 6.47 (d, *J*=2.5 Hz, 1H), 3.87 (s, 3H), 3.78 (s, 4H), 3.64 (s, 2H), 3.46 (s, 2H). ESI-HRMS m/z: calcd for $C_{21}H_{21}NO_5$ $[M-H]^-$ 366.1345, found 366.1349.

Cell viability assay

The cell viability of RPMI-8226 and CZ-1 cells treated with ISL and its derivative **1b** was determined by the MTT (3-(4,5-dimethylthiazol-2-yl)-2,5-diphenyl tetrazolium bromide) assay (Sigma-Aldrich, St. Louis, MO, USA). Tumor cells (5×10^3/well) were seeded in 96-well plates and cultured for 24 h. Then, different concentrations of ISL and **1b** were prepared at the desired concentrations and added into the corresponding plates, in which cells were incubated for an extra 72 h. The RPMI-8226 culture medium with compounds was discarded and 100 µL fresh medium containing 0.5 mg/mL MTT was then added. After 4 h of incubation at 37°C, the solvent was removed and 100 µL dimethyl sulfoxide (DMSO) were added to each well. The absorbance of the each well was measured at 570 nm through SpectraMax M5 Microplate Reader (Molecular Devices, San Jose, CA, USA). The effect of ISL and **1b** on the proliferation of the cells was expressed as IC_{50} value and calculated by using the GraphPad prism 5 software (La Jolla, CA, USA).

Measurement of IL-6 level in CZ-1 cells

CZ-1 cells were seeded into a 96-well plate with the density of 1×10^4/well. ISL and **1b** were added into the corresponding wells at the desired concentrations and incubated for 24 h. RPMI-8226 cell culture medium

was collected, and the IL-6 level in the medium was measured by using enzyme-linked immunosorbent assay (ELISA) kit (Abcam, Cambridge, MA, USA, catalog no. ab46042). The experiments were independently repeated three times.

Western blot

The CZ-1 cells were treated with desired concentrations of ISL (12 μM) and **1b** (1, and 4 μM) for 24 h. The cells were then washed twice with ice-cold PBS and the total cellular protein was extracted by using western blot and IP cell lysis buffer kit (Beyotime, Shanghai, China). Protein concentrations were quantified by using bicinchoninic acid (BCA) Protein Assay Kit (Beyotime, Shanghai, China). Equal amounts of total protein (20 μg) were separated by 12% sodium dodecyl sulfate-polyacrylamide electrophoresis gels (SDS-PAGE) and then transferred onto polyvinylidene fluoride (PVDF) membranes (Millipore, Billerica, MA, USA), blocked with 5% fat-free dry milk / 0.05% Tween 20 at room temperature for 2 h, breezed with the desired primary monoclonal antibodies overnight, which was followed with horseradish peroxidase-conjugated goat anti-rabbit secondary antibody for 1 h. Finally, the immune reactive band was scanned in an electrochemiluminescence (ECL)-detecting reagents (Beyotime, Shanghai, China).

Fluorescence spectroscopy

The fluorescence spectra were recorded on an F-2500 spectrofluorimeter (Hitachi, Tokyo, Japan) equipped with 1.0 cm quartz cells, the widths of both the excitation and emission slits were set the same as 2.5 nm, and the excitation wavelength was 295 nm. Fluorescence spectra were recorded at four different temperatures of 298, 302, 306 and 310 K, respectively, in the range from 300 to 450 nm.

Statistics

Data were reported as mean±SD from three independent experiments, and analyzed using GraphPad Prism version 5.0 (La Jolla, CA, USA) for Windows. Student's t-test was employed for the comparisons between two single groups. Comparison between multiple groups was done using one-way ANOVA test followed by *post hoc* test (Least Significant Difference). P value equal to or less than 0.05 was considered as statistically significant difference.

Results

*Compound **1b** inhibits cancer cells proliferation*

As shown in Figure 2, **1b** is active against RPMI-8226 and CZ-1 cancer cells, with IC_{50} values of 2.04 and 2.97 μM, respectively. In contrast, ISL displayed weaker anti-proliferative activities, with the IC_{50} values 11.6, and 15.5 μM against both cancer cells, respectively.

As shown in Figure 3A, the percentages of apoptotic population of CZ-1 cells treated with 12

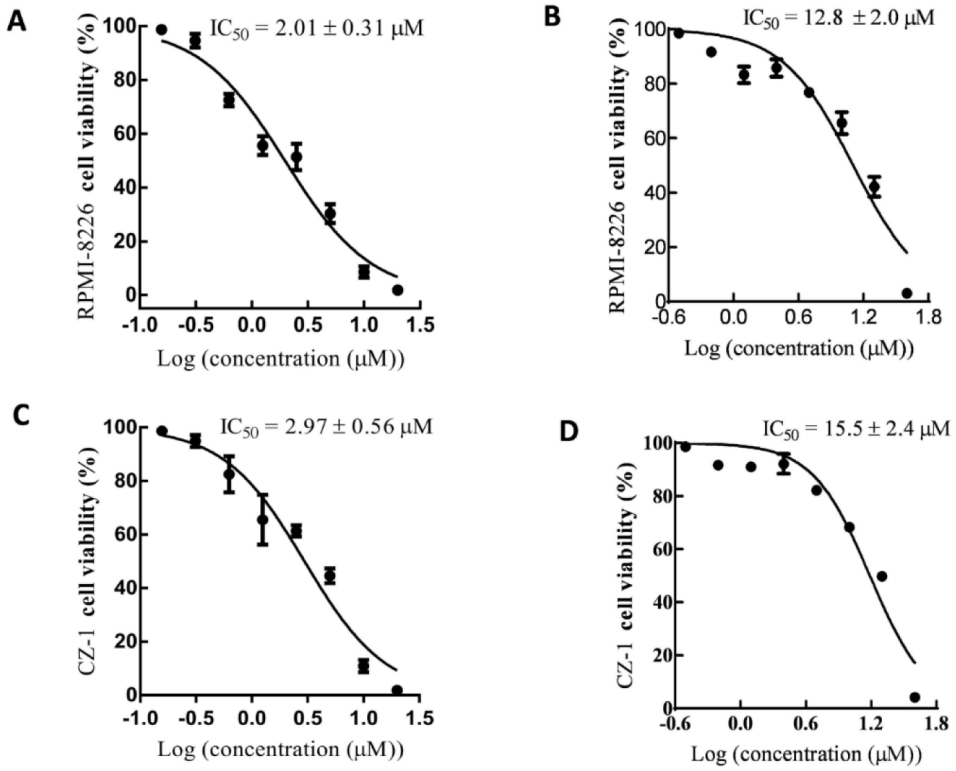

Figure 2. ISL and **1b** inhibit RPMI-8226 and CZ-1 cells proliferation. **(A,B):** ISL and **1b** inhibit RPMI-8226 cells proliferation; **(C,D):** ISL and **1b** inhibit CZ-1 cells proliferation. IC_{50}: inhibitory concentration causing a 50% reduction in cell growth; values are the mean±SD from triplicate cytotoxicity experiments. The positive control drug cis-platinum was used in our experiments, with IC_{50} values of 7.33, and 8.21 μM against RPMI-8226 and CZ-1, respectively.

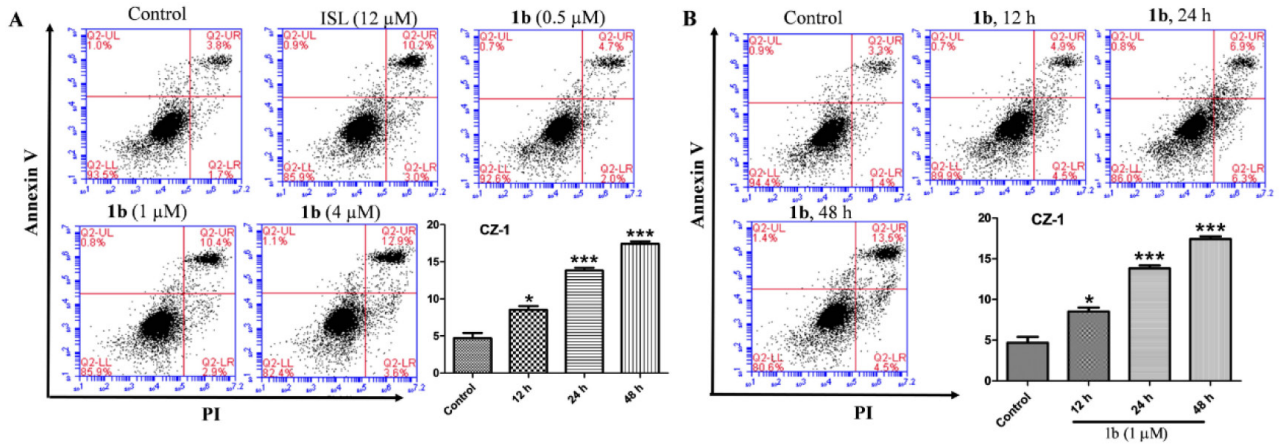

Figure 3. Apoptosis of CZ-1 cells was measured using flow cytometry analysis. **(A):** The cells were treated with ISL (12 μM) and **1b** (0.5, 1, and 4 μM) for 24 h, then were stained with the FITC Annexin V/PI kit. **(B):** The cells were treated with **1b** (1 μM) for 12, 24, and 48 h. The upper right quadrant indicates PI positive/Annexin V positive, late apoptotic or necrotic cells, and cells in the lower right quadrant indicate early apoptotic cells. Bar graph represents statistics of total apoptotic cell percentages from duplicate experiments. *p<0.05 and ***p<0.001 versus control group.

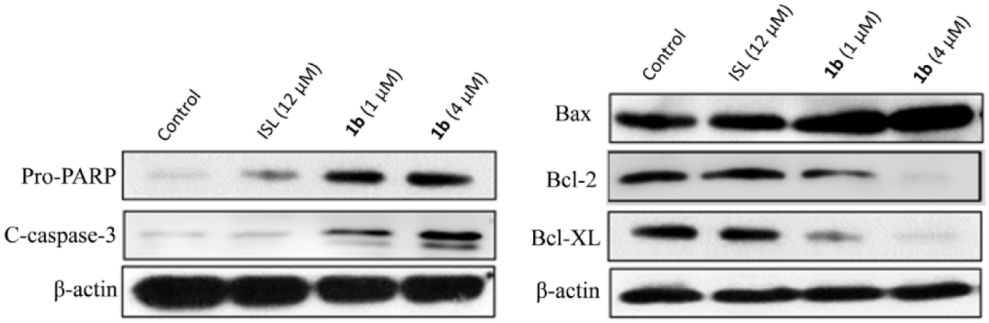

Figure 4. ISL and **1b** induced apoptosis of CZ-1 cells. Cells were treated with ISL and **1b** for 24 h, the levels of the cleavage of the pro-apoptotic proteins PARP, caspase-3, the BCL-2, BCL-xL (anti-apoptotic proteins), and BAX (pro-apoptotic protein) were detected by Western blot. The results indicated that **1b** inhibited cancer cells proliferation.

μM ISL for 24 h was 13.2 %, while for **1b** at 4 μM, clearly outperformed ISL. Moreover, the percentages of apoptosis of CZ-1 cells caused by **1b** at 1 μM for 12, 24, and 48 h were 9.8, 13.7, and 17.8 %, respectively, following a time-dependent manner. In addition, **1b** (1 and 4 μM) induced cleavage of the pro-apoptotic proteins PARP and caspase-3 in CZ-1 cells (Figure 4). We also found that **1b** treatment decreased the protein levels of the anti-apoptotic BCL-2 family proteins, namely BCL-XL and BCL-2, and up-regulated the expression of the apoptotic protein Bax (Figure 4), while ISL at 12 μM failed to induce the same effects, another proof that **1b** is more potent than ISL to inhibit cancer cell proliferation. However, we were also aware that **1b** may inhibit the topoisomerase I activity in cancer cells, similar as ISL [11]. We will report its extensive biological role in our next paper.

*ISL and **1b** reduce the IL-6 expression in cancer cell*

IL-6 is a major growth factor in myeloma cells, playing a key role in the development and regulating cell growth and survival. As shown in Figure 5, **1b** at 4 μM strongly reduced IL-6 expression in CZ-1 cancer cell culture, outperforming ISL at 12 μM.

*Compound **1b** quenches HSA fluorescence emission*

The concentrations of **1b** increased from 0 to 3.0×10^{-5} M with an increment of 0.3×10^{-5} M, while HSA concentration was fixed as 1.0×10^{-5} M. With the addition of **1b**, the fluorescence intensity of HSA was gradually decreased (Figure 6), together with a slight red shift of the emission wavelengths (from 347 to 356), suggesting the formation of a non-fluorescent complex during the binding of **1b** to HSA [20]. The red shift of the emission spectrum could be explained by an increased polarity or a decreased hydrophobicity surrounding the Trp-214 region in HSA [21]. As shown in Figure 6, the emission spectrum of **1b** is the blue trace, which indicates that the free **1b** contributes a negligible fluorescence intensity to HSA emission spectra. The decreased fluorescence intensity

can be described by the Stern-Volmer equation [22]:

$$\frac{F_0}{F} = 1 + K_{SV}[Q]$$

In this equation, F_0 and F are the steady-state fluorescence intensity in the absence and presence of **1b**, [Q] represents the concentration of **1b**, and K_{SV} is the Stern-Volmer quenching constant, which can be obtained from the linear regression of F_0/F versus (Q). Quenching mechanisms can be divided into dynamic quenching or static quenching depending on their temperature and viscosity [23] (Figure 6).

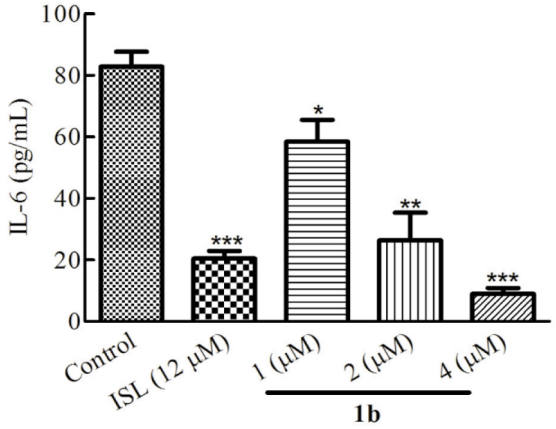

Figure 5. IL-6 level was measured in cell culture medium from CZ-1 control cells, or cells treated with ISL at 12 μM, or **1b** at 1, 2, 4 μM by using human IL-6 ELISA kit. * p<0.05, ** p<0.01, and ***p<0.001 versus the control group.

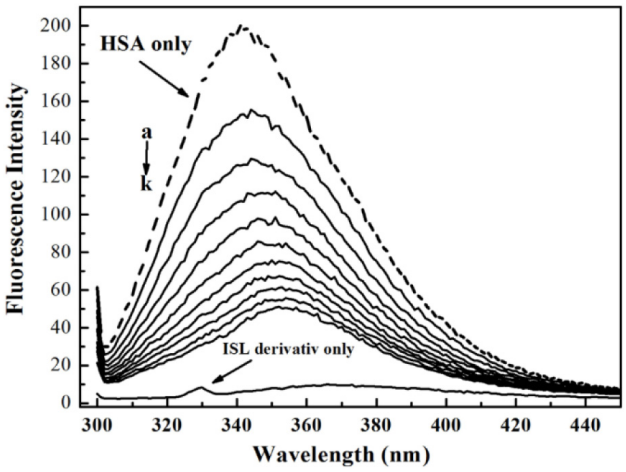

Figure 6. Effect of **1b** on HSA fluorescence spectrum. *c* (HSA)=1.0×10^{-5} M; c (**1b**)/(10^{-5}), *a-j:* from 0.0 M to 3.0 M at an increment of 0.30 M.

Generally, dynamic quenching has enhanced quenching constants with the increasing of temperatures, while in static quenching, the increase in temperatures typically results in smaller quenching constants. According to the Stern-Volmer plots at the tested temperatures, the K_{SV} was calculated (Figure 7A), which were inversely correlated with the increased temperatures (Table 1), indicating the quenching mechanism of the binding interaction by **1b** was static quenching.

Then the Modified Stern-Volmer equation was used to analyze the static quenching procedure of HSA [24]:

$$\frac{F_0}{\Delta F} = \frac{1}{f_a K_a}\frac{1}{[Q]} + \frac{1}{f_a}$$

where ΔF indicated the difference of the fluorescence intensity in the absence and presence of **1b** at the concentration of [Q], K_a refers to the quenching constant for the accessible fluorophores, while f_a represents the fraction of accessible fluorescence. The dependence of $F_0/\Delta F$ on the reciprocal value of concentration $[Q]^{-1}$ is equivalent to the value of $(f_a K_a)^{-1}$. From the equation (Figure 7B), we could calculate the K_a value, which is a very important parameter to decide the free drug concentration in blood.

Small molecule binds to a set of equivalent sites on a macromolecule, the equilibrium binding constant (K_b) and the numbers of binding sites can be obtained from the Scatchard equation [25]:

$$r/D_f = nK_b - rK_b$$

Here, D_f represents the concentration of free small molecule, r is the moles of small molecule binds per mole of protein, n is the binding site multiplicity per class of binding sites. The Scatchard plots are shown in Figure 7C, and the values of K_b and n are listed in Table 1.

Table 1. Quenching, binding constants and thermodynamic parameters of **1b**-HSA system at different Celsius temperatures

T	10^{-4} K_{SV} (L/mol)	10^{-4} K_a (L/mol)	10^{-4} K_b (L/mol)	n	ΔH (kJ×mol^{-1})	ΔG (kJ×mol^{-1})	ΔS
298	8.32	8.25	7.61	1.01	-7.41	-28.05	69.26
302	7.74	8.07	7.33	1.01		-28.33	
306	7.47	7.72	6.85	1.01		-28.61	
310	7.03	7.31	6.32	1.03		-28.88	

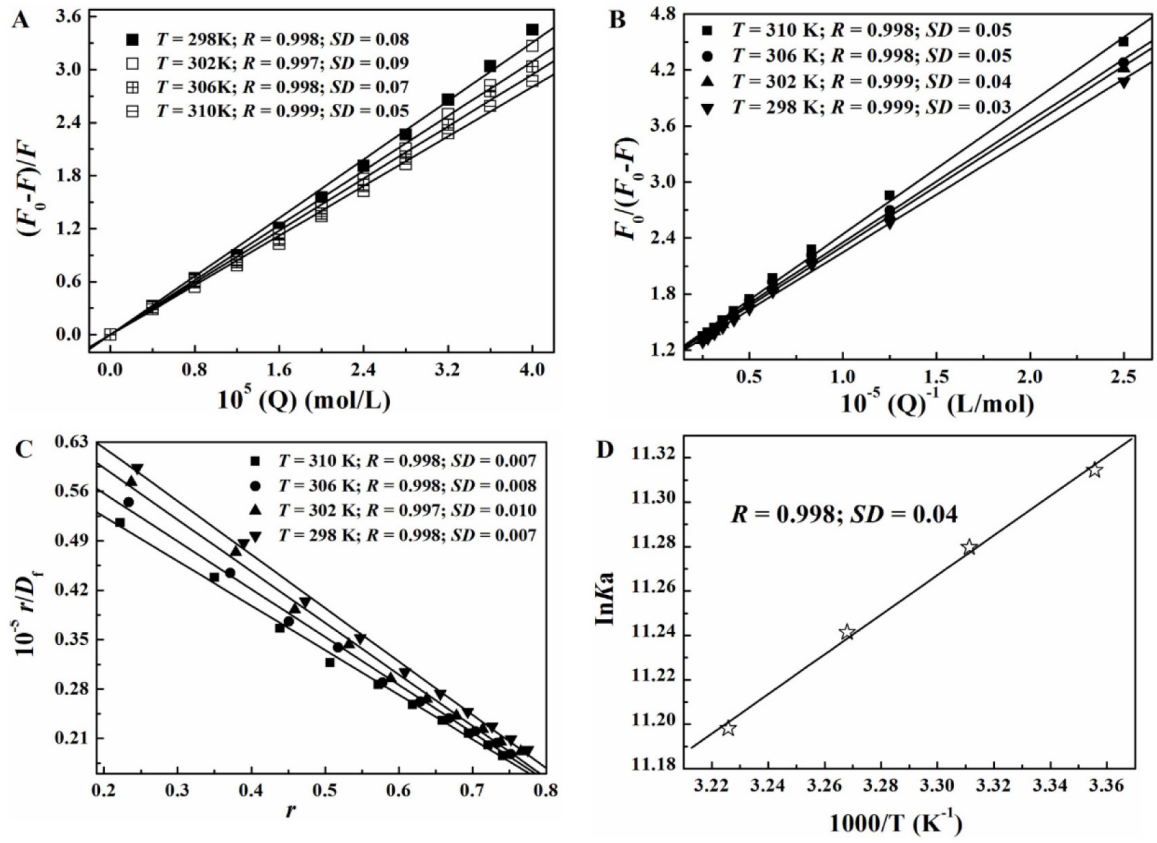

Figure 7. Thermodynamic parameters of **1b** quenches HSA. **(A):** Stern-Volmer plots for quenching the fluorescence of HSA by **1b**; **(B):** Modified Stern-Volmer plots of **1b**-HSA system at different temperatures; **(C):** Scatchard plots for **1b** against HSA; **(D):** Van't Hoff plots of **1b**–HSA system.

As shown in Figure 7B and 7C, the decreasing trend of K_a and K_b with the increasing temperatures was in accordance with K_{SV}'s dependence on temperatures. Usually, drug binds with albumin in blood circulation with an associated complex, and only ~ 1-5% free drug will be available for the biological effects. As shown in Table 1, K_a value is 7.31×10^4 L/mol at 310 K, a moderate binding affinity, indicating a suitable release rate from the protein for **1b**, while for ISL [26], K_a value (5.2×10^4 L/mol, binding with bovine serum albumin) is smaller as compared with **1b**, suggesting ISL may easily be metabolized in the body. The values of the binding site *n* were approximately 1, indicating the interaction of **1b** with HSA has one binding site (Table 1). However, in our site markers competitive experiments, we included **1b** bound to both sites I and II in HSA.

The reversible interaction forces between HSA and drug include van der Waals, electrostatic, hydrogen bond, hydrophobic and steric contacts. In the drug-protein binding process, the changes of entropy (ΔS) and thermodynamic parameter enthalpy (ΔH) are the main evidence to show the interactions between drug and protein. When enthalpy change (ΔH) does not vary significantly over the studied temperatures, which can be calculated from the van't Hoff equation:

$$\ln K_a = -\frac{\Delta H}{RT} + \frac{\Delta S}{R}$$

The K_a is an analogue of the associative binding constants, *R* is the gas constant. Then the thermodynamic parameters (ΔS, ΔH and ΔG) were calculated from the van't Hoff plots. The enthalpy change (ΔH) is estimated from the slope of the van't Hoff relationship. The free energy change (ΔG) is then calculated from the following equation:

$$\Delta G = \Delta H - T\Delta S$$

In Table 1, the negative values of ΔG suggested that the binding process was spontaneous. The negative enthalpy (ΔH) indicated that the binding was mainly enthalpy-driven, and an exothermic reaction may be involved. For the processes involving hydrophobic interactions, the values of ΔS were found to be positive, and the ΔH values were either close to zero or negative. Based on this, the interaction of HSA and **1b** was supposed to be hydrophobic interaction. This seems reasonable, as **1b** possesses a benzenoid character and several non-polar groups, which can interact with HSA's hydrophobic residues. Although an electrostatic

force is also governed by a positive ΔS, the involvement of an electrostatic force in the **1b**-HSA system remains questionable, because **1b** lacks any ionizable group. A negative ΔH also accounts for the involvement of hydrogen bond. Therefore, hydrophobic force and hydrogen bond interaction seem to play the major role in **1b**-HSA interaction [27].

*Identification of the binding site for **1b** on HSA*

To identify which site **1b** binds to HSA, competitive experiments were carried out by using the drugs that specifically bind to the known sites of HSA. Then, the binding behaviors of **1b** to HSA can be monitored by checking the changes in the emission spectrum (Figure 8).

To address the influence of warfarin and ibuprofen on the binding of **1b** to HSA, the binding constants in the presence of site markers were calculated by using the modified Stern-Volmer and Scatchard equations (Figure 8C and 8D). As shown in Table 2, the binding constants were surprisingly variable in the presence of warfarin and ibuprofen. This result indicated that **1b** bounds to HSA on both sites.

Discussion

In this study, we reported an ISL derivative **1b**, which was found to reduce the IL-6 expression in myeloma cells, thus leading to death of malignant cells. To rapidly gain insights into the

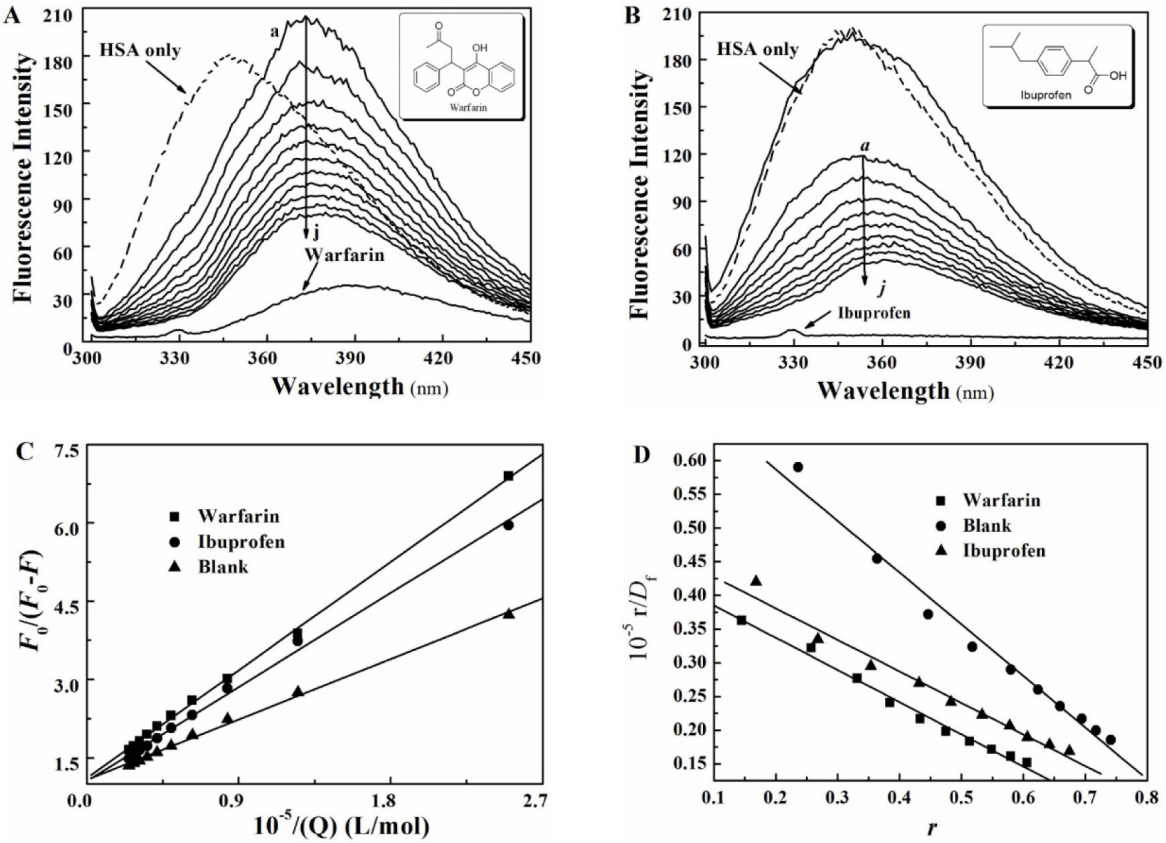

Figure 8. Effect of sites markers on **1b**-HSA system. **(A):** Warfarin effect on the on **1b**-HSA system; **(B):** Ibuprofen effect on the on **1b**-HSA system; **(C):** Modified Stern-Volmer plots of site marker competitive experiments of the **1b**-HSA system; **(D):** Scatchard plots of site marker competitive experiments of the **1b**-HSA system.

Table 2. Binding constants of competitive experiments of **1b**-HSA system (T=310 K)

Site marker	*Modified Stern-Volmer Method*			*Scatchard Method*		
	10^{-4} $K_a/(M^{-1})$	R^a	SD^b	10^{-4} $K_b/(M^{-1})$	R^a	SD^b
(Blank)	8.11	0.997	0.07	7.67	0.991	0.011
Ibuprofen	5.23	0.998	0.09	4.68	0.990	0.012
Warfarin	4.86	0.999	0.05	4.71	0.994	0.007

[a]R is the correlation coefficient; [b]SD is standard deviation

pharmacokinetic property of **1b**, the interactions of **1b** with HSA were studied. **1b** bound to HSA with the binding affinities of the order 10^4 L/mol, showed a moderate binding affinity, suggesting an appropriate free drug concentration for **1b** when transported by the protein. In this experiment, site markers were added equimolar as HSA (1.0×10^{-5} M), **1b** was then gradually added to HSA. As shown in Figure 8, the maximum emission wavelength of HSA had an obvious red shift with the addition of warfarin. Then, the fluorescence intensity of HSA was decreased gradually with the addition of **1b**, accompanying with a slight red shift in the albumin spectrum. This observation demonstrated that the binding of **1b** to HSA was affected by warfarin. Figure 8B showed the changes of the fluorescence emission spectra of **1b**-HSA system in the absence and presence of ibuprofen. By contrast, with the addition of ibuprofen, the emission spectrum of HSA was almost the same [18].

Moreover, the thermodynamic parameters revealed that the binding was characterized by a negative enthalpy (-7.41 $kJ\times mol^{-1}$) and positive entropy changes (69.26 $J\times mol^{-1}\times K^{-1}$), suggesting the binding reaction was exothermic, hydrophobic and hydrogen bond interaction were the predominant intermolecular forces stabilizing HSA-**1b** complex. Site marker competitive experiments demonstrated that **1b** bounds to the sites I and II in HSA.

Conclusions

Our study concluded that **1b** could be transferred by HSA to its target for myeloma cell growth inhibitory effects.

Conflict of interests

The authors declare no conflict of interests.

References

1. Chin YW, Jung HA, Liu Y et al. Anti-oxidant constituents of the roots and stolons of licorice (Glycyrrhiza glabra). J Agric Food Chem 2007;55:4691-7.
2. Peng F, Du Q, Peng C et al. A Review: The Pharmacology of Isoliquiritigenin. Phytother Res 2015;29:969-77.
3. Kong LD, Zhang Y, Pan X, Tan RX, Cheng CH. Inhibition of xanthine oxidase by liquiritigenin and isoliquiritigenin isolated from Sinofranchetia chinensis. Cell Mol Life Sci 2000;57:500-5.
4. Zu M, Yang F, Zhou W, Liu A, Du G, Zheng L. In vitro anti-influenza virus and anti-inflammatory activities of theaflavin derivatives. Antiviral Res 2012;94:217-24.
5. An W, Yang J, Ao Y. Metallothionein mediates cardioprotection of isoliquiritigenin against ischemia-reperfusion through JAK2/STAT3 activation. Acta Pharmacol Sin 2006;27:1431-7.
6. Kim DC, Choi SY, Kim SH et al. Isoliquiritigenin selectively inhibits H(2) histamine receptor signaling. Mol Pharmacol 2006;70:493-500.
7. Kobayashi S, Miyamoto T, Kimura I, Kimura M. Inhibitory effect of isoliquiritin, a compound in licorice root, on angiogenesis in vivo and tube formation in vitro. Biol Pharm Bull 1995;18:1382-6.
8. Ye L, Chan FL, Chen S, Leung LK. The citrus flavonone hesperetin inhibits growth of aromatase-expressing MCF-7 tumor in ovariectomized athymic mice. J Nutr Biochem 2012;23:1230-7.
9. Ding X, Chen H. Anticancer effects of Carvone in myeloma cells is mediated through the inhibition of p38 MAPK signalling pathway, apoptosis induction and inhibition of cell invasion. JBUON 2018;23:747-51.
10. Lu H, Fang ZZ, Cao YF et al. Isoliquiritigenin showed strong inhibitory effects towards multiple UDP-glucuronosyltransferase (UGT) isoform-catalyzed 4-methylumbelliferone (4-MU) glucuronidation. Fitoterapia 2013;84:208-12.
11. Zhao S, Chang H, Ma P et al. Inhibitory effect of DNA topoisomerase inhibitor isoliquiritigenin on the growth of glioma cells. Int J Clin Exp Pathol 2015;8:12577-82.
12. Akilli H, Rahatli S, Tohma YA, Karakas LA, Altundag O, Ayhan A. Effect of increased number of neoadjuvant chemotherapy cycles on tumor resectability and pathologic response in advanced stage epithelial ovarian cancer. JBUON 2018;23:111-15.
13. Gao F, Zhang J, Fu C et al. iRGD-modified lipid-polymer hybrid nanoparticles loaded with isoliquiritigenin to enhance anti-breast cancer effect and tumor-targeting ability. Int J Nanomedicine 2017;12:4147-62.
14. Chen X, Wu Y, Jiang Y et al. Isoliquiritigenin inhibits the growth of multiple myeloma via blocking IL-6 signaling. J Mol Med (Berl) 2012;90:1311-9.
15. Tao P, Li Z, Woolfork AG, Hage DS. Characterization of tolazamide binding with glycated and normal human serum albumin by using high-performance affinity chromatography. J Pharm Biomed Anal 2019;166:273-80.
16. Zhang SL, Damu GL, Zhang L, Geng RX, Zhou CH. Synthesis and biological evaluation of novel benzimidazole derivatives and their binding behavior with bovine serum albumin. Eur J Med Chem 2012;55:164-75.
17. He XM, Carter DC. Atomic structure and chemistry of human serum albumin. Nature 1992;358:209-15.
18. Wanwimolruk S, Birkett DJ, Brooks PM. Structural requirements for drug binding to site II on human serum albumin. Mol Pharmacol 1983;24:458-63.

19. Ibrahim N, Ibrahim H, Kim S, Nallet JP, Nepveu F. Interactions between antimalarial indolone-N-oxide derivatives and human serum albumin. Biomacromolecules 2010;11:3341-351.
20. Rosso SB, Gonzalez M, Bagatolli LA, Duffard RO, Fidelio GD. Evidence of a strong interaction of 2,4-dichlorophenoxyacetic acid herbicide with human serum albumin. Life Sci 1998;63:2343-51.
21. Abou-Zied OK, Al-Lawatia N, Elstner M, Steinbrecher TB. Binding of hydroxyquinoline probes to human serum albumin: combining molecular modeling and Forster's resonance energy transfer spectroscopy to understand flexible ligand binding. J Phys Chem B 2013;117:1062-74.
22. Zhang YZ, Zhou B, Liu YX, Zhou CX, Ding XL, Liu Y. Fluorescence study on the interaction of bovine serum albumin with p-aminoazobenzene. J Fluoresc 2008;18:109-18.
23. Lehrer SS. Solute perturbation of protein fluorescence. The quenching of the tryptophyl fluorescence of model compounds and of lysozyme by iodide ion. Biochemistry-Us 1971;10:3254-63.
24. Ge J, Xing K, Geng X et al. Human serum albumin templated MnO2 nanosheets are oxidase mimics for colorimetric determination of hydrogen peroxide and for enzymatic determination of glucose. Mikrochim Acta 2018;185:559.
25. Li J, Liu X, Ren C, Li J, Sheng F, Hu Z. In vitro study on the interaction between thiophanate methyl and human serum albumin. J Photochem Photobiol B 2009;94:158-63.
26. Chen CB, Chen J, Wang J, Zhu YY, Shi JH. Combined spectroscopic and molecular docking approach to probing binding interactions between lovastatin and calf thymus DNA. Luminescence 2015;30:1004-10.
27. Feroz SR, Mohamad SB, Bujang N, Malek SN, Tayyab S. Multispectroscopic and molecular modeling approach to investigate the interaction of flavokawain B with human serum albumin. J Agric Food Chem 2012;60:5899-5908.